

Carrier-Selective NiO/Si and TiO₂/Si Contacts for Silicon Heterojunction Solar Cells

Hassan Imran, Tarek M. Abdolkader, *Member, IEEE*, and Nauman Z. Butt, *Member, IEEE*

Abstract—Carrier-selective contacts based on thin oxides of nickel and titanium are computationally investigated for heterojunction silicon solar cells. Replacing the standard amorphous/c-Si heterojunction with NiO/c-Si (front) and TiO₂/c-Si (back), we explore the physical requirements to enhance the cell efficiency beyond the physical limits of the conventional structure. Under ideal conditions, a wider bandgap (>3 eV) of these metal oxides provides a high optical transparency, whereas a near-perfect alignment of their energy bands with silicon ensures a high fill factor (FF), which is often difficult to obtain in some of the other wide-bandgap alternatives, e.g., SiO_x, due to imperfect band offsets that hinder carrier extraction. We explore the practical nonidealities that could possibly degrade cell efficiency below its ideal limit. In particular, effects of interfacial defects, Fermi-level pinning at c-Si/TiO₂/metal contact, variability in the bandgap of NiO, and nonoptimized metal oxide doping density are investigated quantitatively. Using the reported experimental data for these nonideal effects, we highlight that the cell efficiency of ~28% could be achieved under AM1.5 illumination with an optimal cell design. These modeling insights provide useful guidelines for the future development of exploratory window layers for silicon solar cells using NiO (front) and TiO₂ (back) heterojunctions.

Index Terms—Carrier-selective contacts, Fermi-level pinning (FLP), heterojunction solar cell, interfacial oxide barrier, quantum tunneling, semiclassical approach.

I. INTRODUCTION

CARRIER-selective contacts are one of the essential requirements for solar cells to operate closer to their thermodynamic limit of maximum efficiency [1]. An ideal selective solar cell contact must fulfill the requirements of high optical transparency, high surface passivation, and low series resistance [2], [3]. Photogenerated carrier loss associated with any of the above-mentioned processes could lead to a significant drop in cell efficiency [4]. The contact selectivity is effectively implemented currently in heterojunction solar cells using amorphous silicon (a-Si) window layers. The most

common example of this is Panasonic's heterojunction with intrinsic thin layer (HIT) solar cell [5], which has recently demonstrated 25.6% record efficiency, the highest by any c-Si solar cell [6].

Despite the remarkably high open-circuit voltages obtained in the HIT structure, a relatively small bandgap (~1.7 eV) of a-Si results in parasitic absorption of photons in the ultraviolet and visible range of the solar spectrum even for a few nanometer thickness of the a-Si layer. Several alternative materials [7]–[11] have been proposed to address the loss of photocurrent in a-Si with some wide-bandgap materials such as molybdenum oxide already showing an impressive progress [12]–[14]. Others include replacing a-Si:H with silicon oxide (a-SiO_x:H) [7], silicon carbide (SiC:H) [9], and III-V compounds (e.g., gallium phosphide [11]). While the replacement of a-Si with a wide bandgap material could provide higher optical transparency and short circuit current density, a loss of FF could often appear, which indicates a reduced carrier extraction. This is attributed to the nonideal energy band offsets [7], [15] at the heterojunctions, which could hinder carrier extraction. The height of these offsets could often deviate from that given by the simple Anderson rule [16] due to interfacial nonidealities such as Fermi-level pinning (FLP), hence requiring process innovations to optimize the carrier extraction.

Recently, Islam and Saraswat [17] have modeled the implementation of NiO/c-Si and TiO₂/c-Si heterojunctions for the carrier selectivity at the front and back contacts, respectively, for silicon solar cells. These oxides have a wide bandgap (>3 eV) and their energy band alignment with c-Si is near-perfect under ideal interfacial conditions for lossless carrier extraction, hence making them worthwhile to be further explored through both experiments and modeling. NiO is a p-type conducting oxide and is found to be highly transparent for 5–10 nm thickness [18]. The reported bandgap of NiO varies between 3.4 and 4.3 eV [18]–[20]. TiO₂ acts as n-type contact with the reported bandgap in the range of 3.2–3.3 eV [21]–[23]. Remarkably, the use of these oxides has been well established as electron/hole extracting layers in organic solar cells, light-emitting diodes, and dye sensitized solar cells [18], [24]–[27]. The use of these oxides for inorganic solar cells has, however, been relatively less explored. There is rarely any experimental demonstration of silicon solar cells with NiO/c-Si heterojunction. TiO₂ contacts have been experimentally reported for silicon solar cells [28] and recently for InP solar cells [29]. While these studies indicate a good potential of these metal oxides for silicon solar cells,

Manuscript received February 12, 2016; revised April 27, 2016 and June 17, 2016; accepted June 22, 2016. Date of publication July 18, 2016; date of current version August 19, 2016. This manuscript was submitted to IEEE Transactions on Electron Devices. The review of this paper was arranged by Editor A. Schenk.

H. Imran and N. Z. Butt are with the Department of Electrical Engineering, School of Science and Engineering, Lahore University of Management Sciences, Lahore 54792, Pakistan (e-mail: hassan.imran.ee@gmail.com; nauman.butt@lums.edu.pk).

T. M. Abdolkader is with the Department of Basic Engineering Sciences, Faculty of Engineering, Benha University, Banha 13511, Egypt. He is now in a leave at the Electrical Engineering Department, Umm Al-Qura University, Makkah 13174, Saudi Arabia (e-mail: tmhasan@uqu.edu.sa).

Color versions of one or more of the figures in this paper are available online at <http://ieeexplore.ieee.org>.

Digital Object Identifier 10.1109/TED.2016.2585523

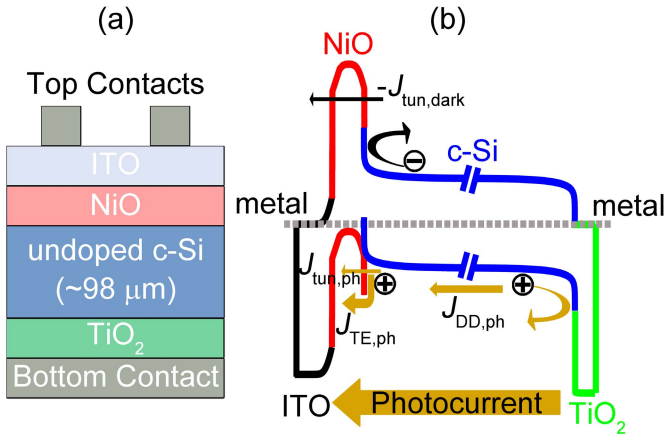


Fig. 1. (a) 2-D schematic of solar cell modeled in this paper. (b) Energy band diagram of the solar cell under short-circuit condition. NiO and TiO₂ layers form heterojunctions with c-Si at the opposite ends and provide selective contacts for holes and electrons, respectively. Various components of dark and photo currents are identified on the band diagram. The diagram is not drawn to scale.

a detailed modeling work is lacking, which could establish the practical limits of these solar cell structures and could guide experimentalists beyond the idealized model of [17].

In this paper, we computationally investigate the design and physics of NiO/c-Si (TiO₂/c-Si) solar cells using self-consistent device simulations. We first establish the ideal limits for the cell characteristics and later explore the effect of nonidealities that could degrade cell efficiency below the ideal limit. In particular, we explore the effects of metal oxide thickness, band offset modulation due to bandgap variation, FLP, metal oxide doping, and interface defect density. All these physical parameters could vary as a function of process/deposition methods and so on, which implies that their role on the cell characteristics needs to be well assessed.

This paper is divided into four sections. Section II describes the modeling approach. Section III discusses the results and the conclusions are provided in Section IV.

II. MODELING APPROACH

A 2-D schematic of the solar cell modeled in this paper is shown in Fig. 1(a). The cell structure consists of intrinsic crystalline silicon (c-Si) as the photoabsorbing material. A thin layer of p-NiO is used for the hole-selective contact, whereas the electron-selective contact is implemented by a thin layer of n-TiO₂. An indium tin oxide (ITO) layer is used at the front contact, while a metal contacts TiO₂ at the back. For simplicity, the metal oxides are considered to be perfectly transparent to the incoming photon spectrum. The device under observation is illuminated with the standard solar spectrum of AM1.5G. Other parameters used for simulations of the cell are listed in Table I and in the Appendix.

A. Cell Electrostatics/Carrier Transport

The energy band diagram of the device under short-circuit condition is shown in Fig. 1(b) along with various components of currents. Photogeneration of carriers takes place inside silicon and a drift-diffusion flux ($J_{DD,ph}$) flows toward the

selective contacts due to the presence of built-in voltage established through p-NiO and n-TiO₂ window layers. At the heterojunctions, the photogenerated carriers could either tunnel ($J_{tun,ph}$) through the metal oxide or go over the energy barrier through thermionic emission ($J_{TE,ph}$). The energy barriers for the interface majority carriers are significantly higher at the heterojunctions due to which the thermionic contribution to the dark current is significantly suppressed. The dark current could, however, flow due to tunneling ($J_{tun,dark}$) and recombination through interface states. We incorporate the mechanisms of carrier transport and cell electrostatics into a unified model, which solves the coupled set of carrier continuity equations and the electrostatics (Poisson equation) self-consistently (see the Appendix). The carrier transport in silicon is solved with drift-diffusion approximation, while the transport mechanisms at the contacts are incorporated as the boundary conditions for the surface velocity in the solution of the coupled Poisson/continuity equations. The numerical solution is performed in 1-D using the simulation tool A Device Emulation Program and Tool (ADEPT) [30].

The charge transport at the contacts (through the metal oxide barriers) is modeled using two complementary approaches. In the first approach, the effect of tunneling and thermionic emission is phenomenologically captured through the surface velocity (v_{surf}) of the carriers at the contacts. Under the limit of zero energy band offset at the heterojunctions, v_{surf} is approximated to be equal to the thermal velocity (v_{th}) of the carriers which for silicon is $\sim 10^7$ cm/s [31]. In the presence of an energy barrier (due to the band offset at the heterojunctions), v_{surf} could be analytically determined using the expression [31], [32]

$$v_{surf} = v_{th}(e^{-\alpha\sqrt{\phi}t_{ox}} + e^{-\phi/k_B T}) \quad (1)$$

where α is the tunneling constant, ϕ is the barrier height, and t_{ox} is the barrier thickness, which in our case is defined by the metal oxide thickness, and given in Å. The first term represents the probability of tunneling using the Wentzel-Kramers-Brillouin (W-K-B) approximation and the second term corresponds to the probability of thermionic emission. In (1), we assume that the carrier recombination through interface traps at the heterojunctions is negligible. This effect is separately discussed in Section II-B.

In the second approach, a numerical solution of quantum tunneling (which could have a dominant contribution for very thin metal oxide thicknesses) is incorporated. In this approach, we have used the transfer matrix method (TMM) [33], [34] for numerically solving the Schrodinger equation, which provides the transmission probability through the thin energy barriers at the contacts. The details of this method have been reported elsewhere [33], [34]. The basic idea of the TMM is to divide the barrier region into small segments such that within each segment the potential is assumed to be constant and, consequently, the wavefunction within each segment is approximated as a plane wave. Applying the conditions of the continuity of the wavefunction and its derivative between each two successive segments, transmission probability as a function of energy is calculated. Comparing the TMM with the conventional finite difference method usually used for

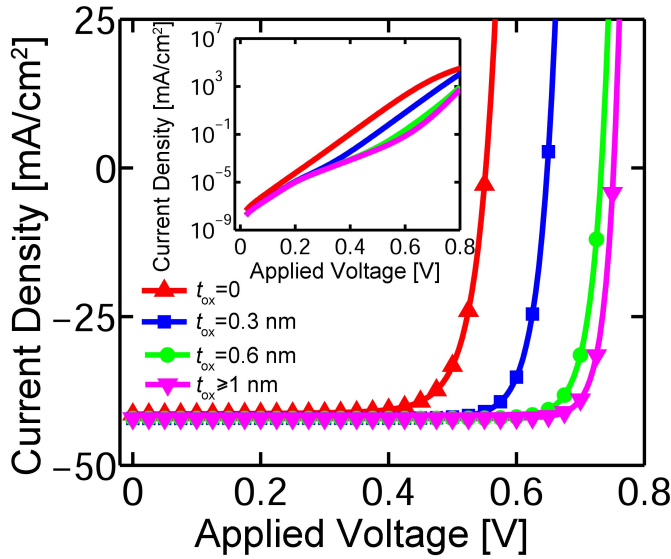


Fig. 2. I - V characteristics of solar cell for a set of oxide thickness. Inset: the I - V characteristics under dark for a set of oxide thickness. The dark saturation current (J_o) remains independent of oxide thickness. The ideality factor (n) increases with increase in oxide thickness and so do V_{oc} and FF.

numerically solving the Schrodinger equation, it has been proved that the TMM has a better accuracy [35].

B. Effect of Surface States

The effect of interfacial defects, which may exist due to the incomplete passivation of silicon surface states at the heterojunctions, is phenomenologically incorporated into the model through v_{surf} . The interfacial defect density (D_{it}) could be analytically expressed as [36]

$$D_{it} = \frac{v_{surf}}{\sigma v_{th} \Delta E} \quad (2)$$

where σ is the capture cross section and is assumed equal to $1 \times 10^{-15} \text{ cm}^{-2}$ [37]. The interfacial defects are assumed to be spread uniformly throughout the energy range (ΔE), which is assumed to be equal to the bandgap of silicon.

C. Effect of Fermi-Level Pinning

It is well known that the metal/semiconductor contacts could exhibit FLP due to penetration of electronic wavefunctions from the metal that creates metal-induced gap states in the semiconductor [38]. The effect of FLP is characterized by pinning factor (S), which is defined as [38]

$$\phi_{M,eff} = S\phi_M + (1 - S)\phi_{CNL} \quad (3)$$

where ϕ_M is the metal workfunction and ϕ_{CNL} is the charge neutrality level in the semiconductor. This effect has been experimentally characterized for Si/TiO₂/metal contacts in the literature [39]. We extract the Schottky barrier height at Si/TiO₂/metal contact by taking a range of S from the experimental data and evaluate its role for the cell characteristics.

III. RESULTS AND DISCUSSION

The current-voltage (I - V) characteristics of the solar cell under illumination are shown in Fig. 2 as a function of oxide

thickness t_{ox} . Perfect band alignment is assumed here, which means that no band offset (energy barrier) exists for interfacial majority carriers at the heterojunctions. High energy band offsets for the interface minority carriers, however, exist due to which the photogenerated carriers going into the wrong contacts are reflected back [see Fig. 1(b)]. This results in slight improvement of short-circuit current density (J_{sc}) for $t_{ox} > 0$. For extremely thin metal oxides ($0 \leq t_{ox} \leq 1 \text{ nm}$), the open-circuit voltage (V_{oc}) shows high sensitivity to t_{ox} and sharply increases as t_{ox} is increased. This behavior is analogous to the typical metal-insulator-semiconductor (MIS) solar cells and is due to the increase in ideality factor (n), as implied by [31]

$$V_{oc} = \frac{nk_B T}{q} \ln \left(\frac{J_{sc}}{J_o} + 1 \right) \quad (4)$$

where n is the ideality factor, q is the charge of electron, and J_o is the dark saturation current density.

The inset in Fig. 2 shows the I - V characteristics under dark as a function of t_{ox} . The increase in n with increasing t_{ox} explains the behavior of V_{oc} in the range $0 \leq t_{ox} \leq 1 \text{ nm}$. For $t_{ox} > 1 \text{ nm}$, n does not change with t_{ox} and correspondingly V_{oc} becomes independent of t_{ox} . It is important to note that J_o is independent of t_{ox} and is limited by the carrier recombination rate in silicon. The latter behavior of V_{oc} is remarkably different compared with the typical MIS solar cells, which shows a rapid degradation in V_{oc} and FF as t_{ox} is increased above an optimal value. In typical MIS solar cells, the energy barriers at the insulator/semiconductor junction are not highly asymmetric. For example, in the metal/SiO₂/c-Si solar cells, which have been extensively investigated since the 1970s, the band offsets for electrons and holes are ~ 3.2 and 4.6 eV , respectively. Under this situation, an increase in t_{ox} above an optimal value (typically 1–2 nm) results in the suppression of photocurrent due to a significant back diffusion of carriers that reflects back from the energy barrier. In contrast, both NiO/c-Si and TiO₂/c-Si heterojunctions, under ideal conditions, do not offer energy barriers for the photocurrent, which allows an unsuppressed flow of photocurrent through thermionic emission even for thicker t_{ox} when the tunneling becomes insignificant.

Having established the ideal characteristics of the cell, we now explore the effect of nonidealities starting with the variability in the bandgap of NiO. The reported values for the NiO bandgap are between 3.4 and 4.3 eV [18]–[20]. Assuming the electron affinity of 1.45 eV [40] for NiO, bandgap greater than $\sim 3.7 \text{ eV}$ for NiO would lower its valence band maximum compared with that of silicon, hence offering an energy barrier (ϕ_{hf}) to the holes at the hole-selective contact. This could bring the cell into a regime where V_{oc} and FF could be affected by the hindrance to the carrier extraction offered by the energy barrier. The solar cell characteristics, i.e., V_{oc} , J_{sc} , FF, and efficiency (η) as a function of t_{ox} , are shown in Fig. 3(a) keeping hole barrier height (ϕ_{hf}) at the front contact fixed at 0.6 eV. The solid and dotted lines represent the results of the semiclassical approach and the quantum mechanical approach, respectively. An excellent match could be observed in the comparison between the two approaches. A significant increase in FF could be observed as t_{ox} increases in the range,

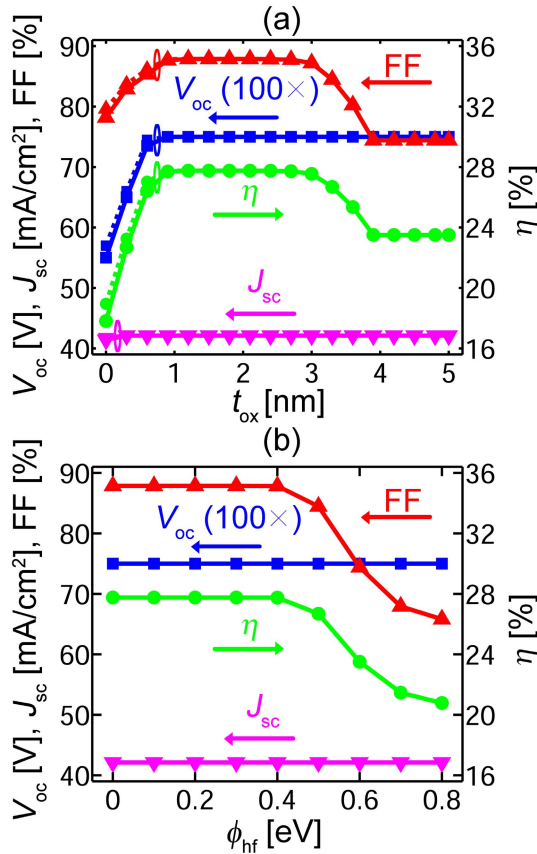


Fig. 3. (a) Open-circuit voltage (V_{oc}), short-circuit current density (J_{sc}), FF, and efficiency (η) as a function of metal oxide thickness (t_{ox}) for hole barrier height (ϕ_{hf}) at the front contact for $\phi_{hf} = 0.6$ eV. The solid lines represent the semiclassical approach where the tunneling probability through rectangular oxide barriers is calculated analytically using the W-K-B approximation for tunneling, whereas the dotted lines represent the quantum mechanical approach to calculate the tunneling of carriers through oxide barrier. For $t_{ox} > 4$ nm, the probability of thermionic emission becomes dominant and solar cell characteristics become independent of oxide thickness. (b) Solar cell characteristics as a function of hole barrier height (ϕ_{hf}) at the front contact for $t_{ox} = 5$ nm. The degradation in FF and η for higher ϕ_{hf} is observed, which indicates a suppression of photogenerated current due to an insufficient probability of thermionic emission. The tunneling of carriers through thicker oxide is negligible for this case.

$0 \leq t_{ox} \leq 1$ nm. This behavior follows the characteristics of V_{oc} in this range of t_{ox} and is typically expected for MIS solar cells [32], [41]. The loss in FF and η for $3 \leq t_{ox} \leq 4$ nm is due to the loss of hole extraction as holes find increasing tunneling resistance with the increase in t_{ox} . The loss of FF saturates for $t_{ox} > 4$ nm when the hole tunneling current becomes negligibly small and the thermionic emission over the oxide barrier becomes the dominant mechanism for hole extraction as described by (1).

The solar cell characteristics are plotted as a function of ϕ_{hf} in Fig. 3(b) keeping the NiO thickness fixed at $t_{NiO} = 5$ nm. For this t_{NiO} , tunneling could be neglected and thermionic emission of holes over the barrier could be assumed as the dominant contribution to the photocurrent. For $\phi_{hf} < 0.4$ eV, the cell characteristics remain essentially unchanged relative to the optimal design that provides efficiency $\sim 28\%$. As ϕ_{hf} is increased above 0.4 eV, the probability of thermionic emission as given by (1) is suppressed to the extent that it affects the extraction of holes. This effect is similar to that of a series

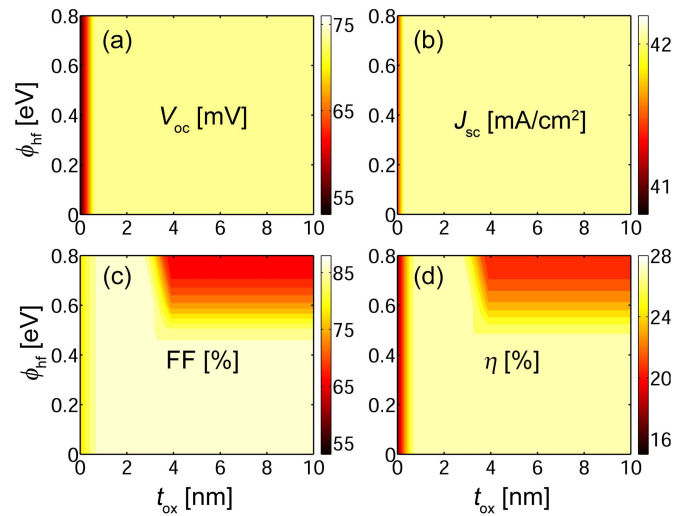


Fig. 4. Solar cell characteristics as a function of oxide thickness (t_{ox}) and hole barrier height (ϕ_{hf}) at the front contact. An optimal design could be achieved for a broad range of t_{ox} (< 1 nm) with $\phi_{hf} \leq 0.5$ eV. For $\phi_{hf} > 0.5$ eV, $t_{ox} \leq 3$ nm is required to avoid the loss in FF.

resistance, which could cause a substantial degradation of FF that could be observed in Fig. 3(b) for $\phi_{hf} > 0.4$ eV. Physically, this suppression of photocurrent represents the situation when the probability of carrier extraction (both tunneling and thermionic emissions) at the contacts becomes low enough so that a substantial carrier density accumulates near the contacts leading to a back diffusion flux from the contacts into the absorber. The observed independence of J_{sc} in the given range of ϕ_{hf} indicates that the back diffusion is significant only under forward bias when the energy bands at the silicon surface become flat enough to support a substantial back diffusion.

The effect of nonideal carrier extraction at the hole-selective contact is further elaborated in the contour plots in Fig. 4, which show the relative effects of t_{NiO} and ϕ_{hf} on cell characteristics. For $t_{NiO} > 1$ nm, the only significant change is observed in FF for $\phi_{hf} > 0.5$ eV. It should be noted that an optimal cell efficiency could be designed by keeping $\phi_{hf} < 0.5$ eV regardless of t_{NiO} . In this optimal regime, the energy barrier at the hole-selective contact remains small enough so that a significant thermionic emission over the barrier could maintain the lossless photocurrent. For $\phi_{hf} > 0.5$ eV, on the other hand, lossless extraction of photocurrent requires $t_{NiO} < 3$ nm so that tunneling could effectively collect the holes, whereas thermionic emission becomes insufficient to support the lossless photocurrent due to relatively high energy barrier. Increasing t_{NiO} above 3 nm for $\phi_{hf} \geq 0.5$ eV results in the carrier extraction loss, which is similar to the effect of series resistance as could be observed in the degradation of the FF in Fig. 4(c). For an extremely thin range of metal oxides ($t_{NiO} \leq 1$ nm), carrier tunneling is the dominant transport mechanism and the typical effects of MIS solar cells are observed. Since the range of bandgap reported for NiO is 3.4–4.3 eV, which represents ϕ_{hf} of 0–0.6 eV, an optimal cell efficiency could therefore be designed for $\phi_{hf} \leq 0.5$ eV without having any first-order dependence on t_{NiO} . It is, however, necessary to ensure $\phi_{hf} < 0.5$ eV to avoid the loss in FF and to maintain the design independency on t_{NiO} .

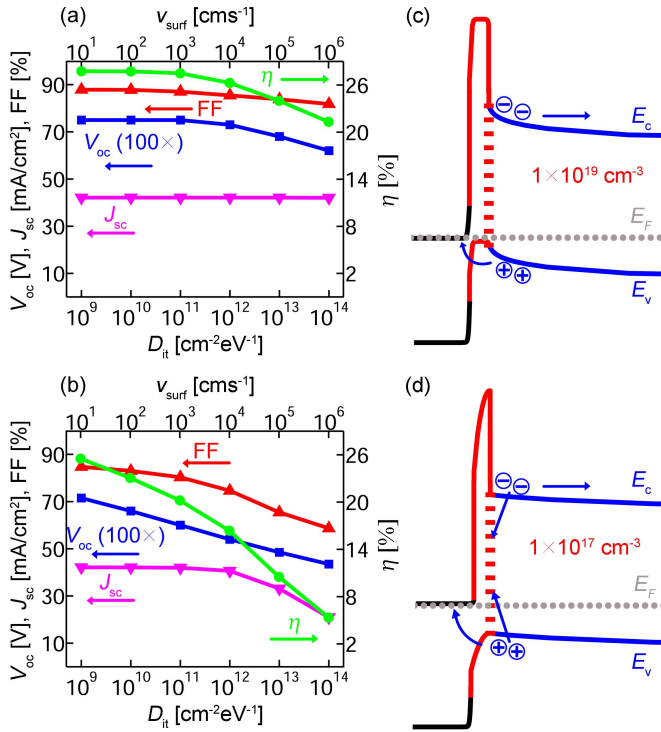


Fig. 5. Solar cell characteristics as a function of interface state density (D_{it}) for different doping densities in NiO ($N_{A,NiO}^-$) of (a) 1×10^{19} and (b) $1 \times 10^{17} \text{ cm}^{-3}$. The higher NiO doping results in a larger V_{bi} and hence a strong electric field at the NiO/Si interface, which lowers the surface recombination for a given D_{it} . Energy band diagrams near the NiO/c-Si interface at short-circuit condition for (c) $N_{A,NiO}^- = 1 \times 10^{19}$ and (d) $N_{A,NiO}^- = 1 \times 10^{17} \text{ cm}^{-3}$. The built-in voltage and the surface electric field for (c) are much higher compared with those for (d). The surface electron density and recombination rate are therefore significantly suppressed for (c) compared with those for (d) for a given value of D_{it} .

Next, we explore the effect of metal oxide doping and the interface trap density (D_{it}) on the cell characteristics. In this regard, two scenarios are considered. In the first case, $N_{A,NiO}^- = 1 \times 10^{19} \text{ cm}^{-3}$ is considered, while in the second case, $N_{A,NiO}^- = 1 \times 10^{17} \text{ cm}^{-3}$ is considered. The solar cell characteristics as a function of D_{it} are plotted for these two cases in Fig. 5(a) and (b), respectively. For $N_{A,NiO}^- = 1 \times 10^{19} \text{ cm}^{-3}$, the cell characteristics essentially remain unaffected by D_{it} for the range of $D_{it} < 10^{11} \text{ cm}^{-2}\text{eV}^{-1}$, whereas the cell degradation starts becoming visible in V_{oc} and FF for $D_{it} > 10^{11} \text{ cm}^{-2}\text{eV}^{-1}$. The cell characteristics for $N_{A,NiO}^- = 1 \times 10^{17} \text{ cm}^{-3}$, on the other hand, show degradation for the D_{it} values as low as $10^9 \text{ cm}^{-2}\text{eV}^{-1}$. The observed behavior could be understood with the energy band diagrams for $N_{A,NiO}^- = 1 \times 10^{19} \text{ cm}^{-3}$ and $N_{A,NiO}^- = 1 \times 10^{17} \text{ cm}^{-3}$, as shown in Fig. 5(c) and (d), respectively. Comparing the two band diagrams, it is evident that higher doping in NiO results in a larger V_{bi} and a stronger energy band bending (that corresponds to strength of electric field) at the NiO/c-Si interface. The higher electric field at the interface is known to lower the interface recombination by lowering the density of photogenerated carriers at the interface. This behavior has been reported earlier for HIT solar cells [42].

Finally, we discuss the effect of FLP at the metal/TiO₂/Si contact. Solar cell characteristics are shown for a range of S

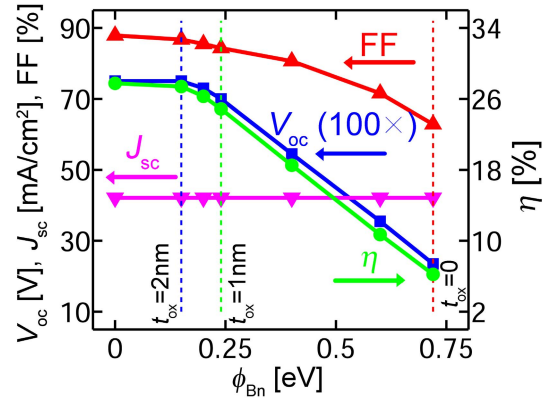


Fig. 6. Solar cell characteristics as a function of Schottky barrier height (ϕ_{Bn}) at Si/TiO₂/metal interface due to FLP. For $\tau_{TiO_2} = 0$ (i.e., silicon/metal contact), V_{oc} and FF drop significantly due to higher ϕ_{Bn} at the interface. As a thin dielectric layer of TiO₂ is inserted between silicon and the metal, the effect of FLP is reduced to a great extent. The dotted lines correspond to ϕ_{Bn} for different TiO₂ layer thicknesses [39].

TABLE I
PARAMETERS USED FOR SOLAR CELL SIMULATIONS

	ITO [44], [45]	NiO	Si	TiO ₂ [46]
Thickness [nm]	100	0–10	9.8×10^4	0–10
E_g [eV]	3.8	3.4–4.3	1.1	3.2–3.3
χ [eV]	4.6	1.45	4.05	4.0
Doping	n-type $E_c = E_F$	p-type ($10^{19}, 10^{17}$) cm^{-3}	Intrinsic	n-type $E_c = E_F$

and the corresponding Schottky barrier height (ϕ_{Bn}) in Fig. 6. For the c-Si/metal contact, i.e., the absence of TiO₂ layer, a significant pinning is experimentally reported [39] with S of 0.075 and ϕ_{Bn} of 0.72 eV [39]. Due to this large ϕ_{Bn} , V_{bi} is substantially reduced resulting in a degraded V_{oc} of ~ 0.24 V. In addition, the FF is also decreased to $\sim 62\%$ for this case resulting in a poor η of $\sim 6\%$. With an addition of a thin (~ 1 nm) TiO₂ layer between c-Si and the metal, the experimental data in [39] show a significant decrease in FLP resulting in $S = 0.24$ and $\phi_{Bn} = 0.24$ eV [39]. For this case, V_{oc} is improved to 0.70 V, the FF is increased to 84% and η is increased to $\sim 25\%$. As the TiO₂ thickness is further increased to 2 nm, ϕ_{Bn} is decreased to 0.15 eV [39]. This improves V_{oc} and the FF to 0.75 V and 86% respectively, giving $\eta = 27.4\%$. Remarkably, this efficiency is very close to that of the best possible case of zero FLP. Further increase in TiO₂ thickness is expected to further reduce ϕ_{Bn} , as reported in [43].

IV. CONCLUSION

We have investigated selective contacts for silicon solar cells using NiO/c-Si (front) and TiO₂/c-Si (back) heterojunctions. Our model incorporates a self-consistent solution of electrostatics and carrier continuity equations. The carrier transport in the silicon is modeled with drift-diffusion approximation,

whereas the quantum mechanical tunneling and thermionic emission are modeled at the contacts using quantum mechanical and semiclassical approaches. Under ideal conditions, the window layers of NiO and TiO₂ provide an excellent alignment of energy bands with c-Si at the heterojunctions, which simultaneously enables high carrier selectivity and lossless extraction of photocurrent at the contacts. Moreover, the wide bandgap (>3 eV) of these metal oxides eliminates the parasitic light absorption associated with standard a-Si/silicon heterojunction solar cells. Practically, an optimal design of these cells, however, requires minimization of several nonideal effects, which could significantly degrade the cell efficiency. In particular, FLP at the metal/TiO₂/Si contact is shown to substantially degrade cell efficiency when the Schottky barrier at this contact exceeds 0.25 eV. The variability in NiO bandgap needs to be limited to ensure a relatively small energy band offset (≤ 0.5 eV) at the hole contact for the lossless carrier extraction. At higher band offsets (>0.5 eV), there could be a loss of photocurrent due to the back diffusion of holes from the contact, unless a very thin metal oxide (<3 nm) is used to support tunneling. An optimal efficiency requires a high doping density (on the order of 10^{19} cm⁻³) in the metal oxides. For an optimal doping of NiO, the surface traps in silicon starts degrading the cell efficiency at trap density above 10^{11} cm⁻²eV⁻¹. The degradation due to surface traps significantly increases as the doping density in NiO is reduced, which is attributed to an enhanced surface recombination due to the lowering of the surface electric field in silicon. With the optimization of nonidealities, the predicted best cell efficiency for these cells is $\sim 28\%$ with a flexible range of oxide thickness. Carefully designed selective contacts based on NiO/TiO₂ could therefore be a potential candidate for commercial heterojunction silicon solar cells.

APPENDIX

The Poisson equation is given by

$$\nabla^2 V(x) = \frac{q}{\epsilon_{\text{Si}}} [N_D - N_A + p(x) - n(x)] \quad (\text{A1})$$

where $V(x)$ is the electrostatic potential, N_D (N_A) is the donor (acceptor) doping density, ϵ_{Si} is the permittivity of silicon, and $n(x)$ and $p(x)$ are position-dependent electron and hole concentrations, respectively. The continuity equation for electrons (holes) is given by

$$\frac{\partial n(p)}{\partial t} = \frac{\pm 1}{q} \nabla \cdot J_{n(p)} + G(x) - R(x) \quad (\text{A2})$$

where $J_{n(p)}$ is the electron (hole) current density, and $G(x)$ and $R(x)$ are carrier generation and recombination rates, respectively. The drift-diffusion equation for electrons (holes) is given by

$$J_{n(p)} = qn(p)\mu_{n(p)} \frac{dV(x)}{dx} \pm qD_{n(p)} \frac{dn(p)}{dx} \quad (\text{A3})$$

where $\mu_{n(p)}$ is the mobility of electrons (holes) and $D_{n(p)}$ is the diffusion constant for electron (hole), respectively.

The back metal workfunction (ϕ_M) is kept at 4.05 eV. The minority carrier lifetimes for electrons and holes in silicon are kept at 30 ms [47]. The radiative recombination

parameter in silicon is set at 1.1×10^{-14} cm³/s [48]. The auger recombination parameters for electrons and holes are set at 1.1×10^{-30} cm⁶/s and at 0.3×10^{-30} cm⁶/s, respectively. The mobilities of electrons and holes in silicon are 1400 cm²/V · s and 400 cm²/V · s, respectively [49]. The effective densities of states in conduction and valance bands are set at 2.86×10^{19} and 3.10×10^{19} cm⁻³, respectively [50].

ACKNOWLEDGMENT

The authors would like to thank M. Ahmad for his fruitful discussions. They would also like to thank Y. Jahngger for his valuable comments and suggestions to improve the quality of this paper.

REFERENCES

- [1] W. Shockley and H. J. Queisser, "Detailed balance limit of efficiency of p-n junction solar cells," *J. Appl. Phys.*, vol. 32, no. 3, pp. 510–519, 1961.
- [2] D. L. Young, W. Nemeth, S. Grover, A. Norman, B. G. Lee, and P. Stradins, "Carrier-selective, passivated contacts for high efficiency silicon solar cells based on transparent conducting oxides," in *Proc. IEEE 40th Photovolt. Specialist Conf. (PVSC)*, Jun. 2014, pp. 1–5.
- [3] J. Bullock *et al.*, "Amorphous silicon passivated contacts for diffused junction silicon solar cells," *J. Appl. Phys.*, vol. 115, no. 16, p. 163703, 2014.
- [4] R. M. Swanson, "Approaching the 29% limit efficiency of silicon solar cells," in *Proc. Conf. Rec. 31st IEEE Photovolt. Specialists Conf.*, Jan. 2005, pp. 889–894.
- [5] M. Taguchi, A. Terakawa, E. Maruyama, and M. Tanaka, "Obtaining a higher V_{oc} in HIT cells," *Prog. Photovolt.*, vol. 13, no. 6, pp. 481–488, 2005.
- [6] K. Masuko *et al.*, "Achievement of more than 25% conversion efficiency with crystalline silicon heterojunction solar cell," *IEEE J. Photovolt.*, vol. 4, no. 6, pp. 1433–1435, Nov. 2014.
- [7] J. P. Seif *et al.*, "Amorphous silicon oxide window layers for high-efficiency silicon heterojunction solar cells," *J. Appl. Phys.*, vol. 115, no. 2, p. 024502, 2014.
- [8] C. Battaglia *et al.*, "Hole selective MoO_x contact for silicon solar cells," *Nano Lett.*, vol. 14, no. 2, pp. 967–971, 2014.
- [9] P. Stradins *et al.* (Dec. 2014.) *Passivated Tunneling Contacts to N-Type Wafer Silicon and Their Implementation into High Performance Solar Cells: Preprint*. [Online]. Available: <http://www.osti.gov/scitech/servlets/purl/1166658>
- [10] S. De Wolf, A. Descoedres, Z. C. Holman, and C. Ballif, "High-efficiency silicon heterojunction solar cells: A review," *Green*, vol. 2, no. 1, pp. 7–24, 2012.
- [11] S. Limpert *et al.*, "Results from coupled optical and electrical sentaurus TCAD models of a gallium phosphide on silicon electron carrier selective contact solar cell," in *Proc. IEEE 40th Photovolt. Specialist Conf. (PVSC)*, Jun. 2014, pp. 0836–0840.
- [12] J. Geissbühler *et al.*, "22.5% efficient silicon heterojunction solar cell with molybdenum oxide hole collector," *Appl. Phys. Lett.*, vol. 107, no. 8, p. 081601, 2015.
- [13] J. Bullock, C. Samundsett, A. Cuevas, D. Yan, Y. Wan, and T. Allen, "Proof-of-concept p-type silicon solar cells with molybdenum oxide local rear contacts," *IEEE J. Photovolt.*, vol. 5, no. 6, pp. 1591–1594, Nov. 2015.
- [14] M. Bivour, J. Temmler, H. Steinkemper, and M. Hermle, "Molybdenum and tungsten oxide: High work function wide band gap contact materials for hole selective contacts of silicon solar cells," *Solar Energy Mater. Solar Cells*, vol. 142, pp. 34–41, Nov. 2015.
- [15] C. Battaglia *et al.*, "Silicon heterojunction solar cell with passivated hole selective MoO_x contact," *Appl. Phys. Lett.*, vol. 104, no. 11, p. 113902, 2014.
- [16] R. L. Anderson, "Germanium-gallium arsenide heterojunctions," *IBM J. Res. Develop.*, vol. 4, no. 3, pp. 283–287, Jul. 1960.
- [17] R. Islam and K. C. Saraswat, "Metal/insulator/semiconductor carrier selective contacts for photovoltaic cells," in *Proc. IEEE 40th Photovolt. Specialist Conf. (PVSC)*, Jun. 2014, pp. 0285–0289.

- [18] M. D. Irwin, D. B. Buchholz, A. W. Hains, R. P. H. Chang, and T. J. Marks, "p-Type semiconducting nickel oxide as an efficiency-enhancing anode interfacial layer in polymer bulk-heterojunction solar cells," *Proc. Nat. Acad. Sci. USA*, vol. 105, no. 8, pp. 2783–2787, 2008.
- [19] S. Hüfner, "Electronic structure of NiO and related 3D-transition-metal compounds," *Adv. Phys.*, vol. 43, no. 2, pp. 183–356, 1994.
- [20] P. S. Patil and L. D. Kadam, "Preparation and characterization of spray pyrolyzed nickel oxide (NiO) thin films," *Appl. Surf. Sci.*, vol. 199, nos. 1–4, pp. 211–221, 2002.
- [21] S. Sen, S. Mahanty, S. Roy, O. Heintz, S. Bourgeois, and D. Chaumont, "Investigation on sol-gel synthesized Ag-doped TiO₂ cermet thin films," *Thin Solid Films*, vol. 474, nos. 1–2, pp. 245–249, 2005.
- [22] Z. Wang, U. Helmerrsson, and P.-O. Käll, "Optical properties of anatase TiO₂ thin films prepared by aqueous sol-gel process at low temperature," *Thin Solid Films*, vol. 405, nos. 1–2, pp. 50–54, 2002.
- [23] P. Chrysicopoulou, D. Davazoglou, C. Trapalis, and G. Kordas, "Optical properties of very thin (<100 nm) sol-gel TiO₂ films," *Thin Solid Films*, vol. 323, no. 1, pp. 188–193, 1998.
- [24] J. Wang *et al.*, "Performance enhancement of perovskite solar cells with Mg-doped TiO₂ compact film as the hole-blocking layer," *Appl. Phys. Lett.*, vol. 106, no. 12, p. 121104, 2015.
- [25] H. Huang *et al.*, "Improved and orange emission from an n-ZnO/p-Si heterojunction light emitting device with NiO as the intermediate layer," *Appl. Phys. Lett.*, vol. 101, no. 22, p. 223504, 2012.
- [26] Y. Zhao *et al.*, "Study on the electroluminescence properties of diodes based on n-ZnO/p-NiO/p-Si heterojunction," *Opt. Commun.*, vol. 336, pp. 1–4, Feb. 2015.
- [27] D. Gebeyehu *et al.*, "Hybrid solar cells based on dye-sensitized nanoporous TiO₂ electrodes and conjugated polymers as hole transport materials," *Synth. Met.*, vol. 125, no. 3, pp. 279–287, 2001.
- [28] S. Avasthi, W. E. McClain, G. Man, A. Kahn, J. Schwartz, and J. C. Sturm, "Hole-blocking titanium-oxide/silicon heterojunction and its application to photovoltaics," *Appl. Phys. Lett.*, vol. 102, no. 20, p. 203901, 2013.
- [29] X. Yin *et al.*, "19.2% efficient InP heterojunction solar cell with electron-selective TiO₂ contact," *ACS Photon.*, vol. 1, no. 12, pp. 1245–1250, 2014.
- [30] J. Gray, X. Wang, R. V. K. Chavali, X. Sun, A. Kanti, and J. R. Wilcox. (Mar. 2016). *ADEPT 2.1*. [Online]. Available: <https://nanohub.org/resources/adeptnpt>
- [31] S. M. Sze and K. K. Ng, *Physics of Semiconductor Devices*. Hoboken, NJ, USA: Wiley, 2006.
- [32] H. Imran and N. Z. Butt, "Computational study of hybrid nanomaterial/insulator/silicon solar cells," *IEEE Trans. Electron Devices*, vol. 62, no. 10, pp. 3111–3116, Oct. 2015.
- [33] T. M. Abdolkader, "A new approach for numerical simulation of quantum transport in double-gate SOI," *Int. J. Numer. Model., Electron. Netw., Devices Fields*, vol. 20, no. 6, pp. 299–309, 2007.
- [34] T. M. Abdolkader, H. H. Hassan, W. Fikry, and O. A. Omar, "Solution of Schrödinger equation in double-gate MOSFETs using transfer matrix method," *Electron. Lett.*, vol. 40, no. 20, pp. 1307–1308, Sep. 2004.
- [35] T. M. Abdolkader, W. F. Farouk, O. Omar, and M. F. M. Hassan, "FETMOSS: A software tool for 2D simulation of double-gate MOSFET," *Int. J. Numer. Model., Electron. Netw., Devices Fields*, vol. 19, no. 4, pp. 301–314, 2006.
- [36] R. F. Pierret, *Advanced Semiconductor Fundamentals*, vol. 6. Upper Saddle River, NJ, USA: Prentice-Hall, 2003.
- [37] E. Yablonovitch, D. L. Allara, C. C. Chang, T. Gmitter, and T. B. Bright, "Unusually low surface-recombination velocity on silicon and germanium surfaces," *Phys. Rev. Lett.*, vol. 57, no. 2, p. 249, 1986.
- [38] J. Robertson, "Band offsets of wide-band-gap oxides and implications for future electronic devices," *J. Vac. Sci. Technol. B*, vol. 18, no. 3, pp. 1785–1791, 2000.
- [39] A. Agrawal *et al.*, "Fermi level depinning and contact resistivity reduction using a reduced titania interlayer in n-silicon metal-insulator-semiconductor ohmic contacts," *Appl. Phys. Lett.*, vol. 104, no. 11, p. 112101, 2014.
- [40] H. Wu and L.-S. Wang, "A study of nickel monoxide (NiO), nickel dioxide (ONiO), and Ni(O₂) complex by anion photoelectron spectroscopy," *J. Chem. Phys.*, vol. 107, no. 1, pp. 16–21, 1997.
- [41] M. A. Green, *Solar Cells: Operating Principles, Technology, and System Applications*. Englewood Cliffs, NJ, USA: Prentice-Hall, 1982.
- [42] A. Datta, M. Rahmouni, M. Nath, R. Boubekri, P. R. I. Cabarrocas, and P. Chatterjee, "Insights gained from computer modeling of heterojunction with intrinsic thin layer 'HIT' solar cells," *Solar Energy Mater. Solar Cells*, vol. 94, no. 9, pp. 1457–1462, 2010.
- [43] B.-Y. Tsui and M.-H. Kao, "Mechanism of Schottky barrier height modulation by thin dielectric insertion on n-type germanium," *Appl. Phys. Lett.*, vol. 103, no. 3, p. 032104, 2013.
- [44] B. Höffling, A. Schleife, F. Fuchs, C. Rödl, and F. Bechstedt, "Band lineup between silicon and transparent conducting oxides," *Appl. Phys. Lett.*, vol. 97, no. 3, p. 032116, 2010.
- [45] A. Klein, "Electronic properties of In₂O₃ surfaces," *Appl. Phys. Lett.*, vol. 77, no. 13, p. 2009, 2000.
- [46] I. Jögi, K. Kukli, M. Kemell, M. Ritala, and M. Leskelä, "Electrical characterization of Al_xTi_yO_z mixtures and Al₂O₃-TiO₂-Al₂O₃ nanolaminates," *J. Appl. Phys.*, vol. 102, no. 11, p. 114114, 2007.
- [47] A. Cuevas and D. Macdonald, "Measuring and interpreting the lifetime of silicon wafers," *Solar Energy*, vol. 76, nos. 1–3, pp. 255–262, 2004.
- [48] W. Gerlach, H. Schlagenotto, and H. Maeder, "On the radiative recombination rate in silicon," *Phys. Status Solidi A*, vol. 13, no. 1, pp. 277–283, 1972.
- [49] C. Jacoboni, C. Canali, G. Ottaviani, and A. A. Quaranta, "A review of some charge transport properties of silicon," *Solid-State Electron.*, vol. 20, no. 2, pp. 77–89, 1977.
- [50] M. A. Green, "Intrinsic concentration, effective densities of states, and effective mass in silicon," *J. Appl. Phys.*, vol. 67, no. 6, pp. 2944–2954, 1990.

Authors' photographs and biographies not available at the time of publication.